RSC Advances

REVIEW

View Article Online
View Journal | View Issue

Cite this: *RSC Adv.*, 2022, **12**, 1433

Metal–organic frameworks (MOFs) based nanofiber architectures for the removal of heavy metal ions

Heja Ibrahim Adil,[a] Mohammad R. Thalji,[f] Suhad A. Yasin,[a] Ibtisam A. Saeed,[a] Mohammed A. Assiri,[cd] Kwok Feng Chong[b] and Gomaa A. M. Ali *[e]

Environmental heavy metal ions (HMIs) accumulate in living organisms and cause various diseases. Metal–organic frameworks (MOFs) have proven to be promising and effective materials for removing heavy metal ions from contaminated water because of their high porosity, remarkable physical and chemical properties, and high specific surface area. MOFs are self-assembling metal ions or clusters with organic linkers. Metals are used as dowel pins to build two-dimensional or three-dimensional frameworks, and organic linkers serve as carriers. Modern research has mainly focused on designing MOFs-based materials with improved adsorption and separation properties. In this review, for the first time, an in-depth look at the use of MOFs nanofiber materials for HMIs removal applications is provided. This review will focus on the synthesis, properties, and recent advances and provide an understanding of the opportunities and challenges that will arise in the synthesis of future MOFs–nanofiber composites in this area. MOFs decorated on nanofibers possess rapid adsorption kinetics, a high adsorption capacity, excellent selectivity, and good reusability. In addition, the substantial adsorption capacities are mainly due to interactions between the target ions and functional binding groups on the MOFs–nanofiber composites and the highly ordered porous structure.

Received 19th September 2021
Accepted 8th December 2021

DOI: 10.1039/d1ra07034g

rsc.li/rsc-advances

[a]*College of Science, University of Duhok, Duhok, 42001, Iraq*
[b]*Faculty of Industrial Sciences & Technology, Universiti Malaysia Pahang, Gambang, 26300 Kuantan, Malaysia*
[c]*Research Center for Advanced Materials Science (RCAMS), King Khalid University, Abha, Kingdom of Saudi Arabia*
[d]*Department of Chemistry, Faculty of Science, King Khalid University, P.O. Box 9004, Abha 61413, Saudi Arabia*
[e]*Chemistry Department, Faculty of Science, Al-Azhar University, Assiut 71524, Egypt. E-mail: gomaasanad@azhar.edu.eg*
[f]*Independent Researcher, Amman, Jordan*

Heja Ibrahim Adil graduated from the University of Duhok, College of Science, Department of Chemistry in the academic year 2010–2011. She worked as a teaching assistant until the year 2020 at the University of Duhok, Kurdistan region, Iraq, before being accepted for post-graduate studies (masters student) in February 2020 to study Inorganic Chemistry.

Dr Mohammad R. Thalji received his Bachelor of Science in Applied Chemistry from Tafila Technical University, Jordan (2006) and his Master of Science in Chemistry from Yarmouk University, Jordan (2011). He then worked as a chemistry lecturer at Shaqra University, Kingdom of Saudi Arabia. In September 2017, he started his PhD study at the University Malaysia Pahang under the supervision of Prof. Chong Kwok Feng and received his PhD in Physical Chemistry (Advanced Materials & Nanotechnology) in September 2020. His research focuses on the development of novel nanomaterial-based devices for energy storage (supercapacitors and batteries) and water treatment applications. Dr Thalji is an executive editor and editorial board member for many international journals, as well as a reviewer for several journals.

1. Introduction

Heavy metal ions (HMIs) are the most common environmental pollutants found in water sources. Toxic HMIs with densities above 5 g cm^{-3} in water, including arsenic (As), lead (Pb), mercury (Hg), cobalt (Co), chromium (Cr), copper (Cu), cadmium (Cd), antimony (Sb), and uranium (U), are considered pollutants and represent a significant global problem.[1,2] Owing to their incorporation into the atmosphere, these ions are hazardous and harmful to human health.[3] The HMIs in aquatic life can damage the foundations of life, especially the food system.[4] As a result, their removal has become a major requirement.[5] Most of these HMIs are present in the cationic form in water (M^{n+}), and some of them are present in the anionic form, such as As (arsenate AsO_4^{3-}, arsenite AsO_3^{3-}),[6] and Cr (in which $HCrO_4^-$ and $Cr_2O_7^{2-}$ are the main forms for Cr(VI) below pH = 3).[6] Many strategies have been used to remove HMIs from water, including nanofiltration,[7] solvent extraction and ion exchange,[8,9] the use of resins,[10] photocatalytic degradation,[11,12] chemical precipitation, ion exchange, cooling, chemical deposition, biological treatment, reverse osmosis, and adsorption.[4,13–16] Adsorption is one of the most effective treatment strategies as it does not require high temperatures and can simultaneously adsorb many chemicals.[12,17,18] Activated carbon (AC), clay minerals, chitosan, and bi-layer hydroxides are among the porous natural resource materials that have been reported.[19–21] However, these materials show poor processing and selectivity. On the other hand, it is generally insufficient from a social, ecological, and commercial point of view.[22] For example, some metal ions oxidize and dissolve porous adsorbents containing organic acids, such as organic synthetic polymers, leading to secondary pollutants and, more importantly, the inability to achieve a low representation of metal ions. Therefore, to overcome these difficulties and limitations, a liquid is required.

Metal–organic frameworks (MOFs) are low-density crystalline structures containing metal ion units or clusters to form compounds and they have recently attracted significant interest.[13,23] The hydro (solvo) thermal, mechanochemical, sonochemical, electrochemical, layer-by-layer development, and micro-processing methods can enable processing of these compounds at temperatures up to 220 °C and low air pressures

Suhad Yasin is a PhD lecturer at the University of Duhok, Kurdistan region, Iraq. She received her Master's degree in Chemistry/Polymer Chemistry in 2009. During her Master's studies (2007–2009), she had published many articles focused on preparing new materials for removing heavy metals from aqueous solutions. Since October 2016, her research activities have mainly centered on the preparation of nanofibers to treat water contaminated with hazardous materials. She received her PhD degree in 2020 from the University of Duhok. She is also a principal investigator at Partnerships for Enhanced Engagement in Research (PEER) under Cycle 6/IRAQ. This project is focused on studying the functions of nanofiber membranes and their use to remove heavy metals from aqueous solutions.

Ibtisam Saeed, 66 years old, is a lecturer in the Physics Department, College of Science, University of Duhok, Iraq. She obtained a PhD in Physics/Electronics from the University of California in 1982. She also obtained her MSc in Physics from the University of California at 1979. Before that, she obtained a BSc in Physics from Baghdad University at 1974. After passing her BSc degree, she worked as a teaching assistant at the University of Baghdad. After completing her PhD degree, she worked as scientific researcher, and then a senior scientific researcher at the Iraqi Atomic Energy Organization, (1982–1991), in the field of automated system design. She designed and implemented many control and data acquisition (DAQ) systems, hardware and software. After 1991, she transferred to the Military Industrial Corporation, General Company for Mechanical and Electronic designs as a senior scientific researcher, and the head of senior researchers (1991–2003), where she participated in projects on the reconstruction of electrical power plants and worked in the field of reverse engineering. After 2003, she moved to the Electronic Systems Centre, Ministry of Manufacturing and Minerals, as a head of senior researchers, and then expert (2003–2005). Many monitoring and DAQ systems have been designed and implemented by her group. In 2005, she began working as a university lecturer at University of Duhok, College of Science, Department of Physics. She is a now a member of the UoD PEER project group, working in the field of nanotechnology, she began working in this field by designing and implementing an electrospinning device.

with a pH in the range of 1 to 10.[24] Element modules and organic linkers can be combined in an infinite number of ways to create novel structures with fascinating properties for various applications, such as heterogeneous catalysis and photocatalysis,[25] drug delivery,[26] energy collection,[27] gas storage,[28] sensing,[29] adsorption,[30] and the identification of dangerous chemicals.[31]

MOFs-based materials are effective adsorbents for HMIs removal owing to their large surface areas, good physicochemical properties, high porosity, and intelligent structure[32]. MOFs can be employed directly as heavy metal ion (HMI) adsorbents. However, the organic ligands in pure MOFs usually lack active functional groups, which leads to an inadequate adsorption capability. For example, MIL-100(Fe) could remove Pb(II) and Cd(II) with an adsorption capacity of 28.29 and 8.79 mg g^{-1}, respectively.[33] Various formulations of MOFs materials, such as composite beads, are used to remove HMIs owing to the tunable nature of MOFs. Boix *et al.*[34] reported microbead composites obtained by incorporating inorganic nanoparticles into MOFs (CeO_2@UiO-66 and CeO_2@UiO-66-$(SH)_2$) for the removal of various metals from water, including As(III) and Cr(VI), with a 31% and 68% adsorption efficiency, respectively. In another work, the adsorption performance of Pb(II) in an aqueous solution was assessed by Jin *et al.* using carboxymethyl cellulose–coated metal–organic material (MOF-5–CMC) as a possible adsorbent with a 79% adsorption efficiency within 120 min at an optimal pH of 5–6.[35]

Metal organic framework (MOF) and nanofiber designs have been combined in recent years to improve the overall performance of MOF–nanofiber composites structures for the removal of HMIs.[36] MOFs nanofibers have a high porosity, a large specific surface area, and numerous active sites, making them ideal for the adsorption of HMIs. MOF nanoparticles can also form on the nanofiber substrate, reducing aggregation and exposing additional adsorption sites. In addition, their membranes offer the advantages of flexibility and a high loading capacity. Owing to their organic–inorganic nature and low density, MOFs are more compatible with polymer fibers than other MOF-based composites, including metals, metal

Dr Gomaa A. M. Ali is an Associate Professor at the Chemistry Department, Faculty of Science, Al-Azhar University, Egypt. He has 15 years of experience research the fields of materials science, nanocomposites, humidity sensing, graphene, supercapacitors, water treatment, and drug delivery. He was awarded his PhD in Advanced Nanomaterials for Energy Storage from UMP, Malaysia. He is the recipient of some national and international prizes and awards, such as TWAS-AREP (2018), Obada International Prize (2021), Gold Medal (Archimedes, Russia, 2014), Green Technology Award (CITREX, Malaysia, 2015), and the Gold Medal (British Invention Show, UK, 2015). He has published over 112 journal articles and 16 book chapters on a broad range of cross disciplinary research fields, including supercapacitors, water treatment, humidity sensing, biosensing, corrosion, and drug delivery. To date, he has more than 2995 citations and an h-index of 32. He has served as an editor for many international journals and a reviewer for more than 60 WoS journals. He is a member of national and international scientific societies, such as the American Chemical Society (ACS) and the Egyptian Young Academy of Sciences (EYAS). He is an editor for the handbook "Waste recycling technologies for nanomaterials manufacturing" Springer, 2021.

Dr Mohammed A. Assiri is the head of the Chemistry Department, College of Science, King Khalid University, Abha, KSA. He obtained his PhD in Organic Chemistry and Green Chemistry, December 2016, from the University of Wyoming, Laramie, WY, USA, and his Masters of Science in Organic Chemistry in April 2014 from the University of Wyoming, Laramie, WY, USA. His research experience includes UV-vis spectra, nuclear magnetic resonance (NMR) spectroscopy, fluorescence lifetimes, mass spectrometry, X-ray diffraction, TA Instruments SDT Q600 thermogravimetric analysis (TGA), Brunauer–Emmet–Teller analysis (BET), Fourier transform infrared (FTIR) spectroscopy, and scanning electron microscopy (SEM). He is the co-author of many journal articles and has also obtained some awards.

Dr Kwok Feng Chong received his first class honors BSc. Degree in Industrial Chemistry from Universiti Teknologi Malaysia in 2004. He pursued his postgraduate studies in the field of chemistry and obtained a PhD from the National University of Singapore in 2010. Presently, he is a full professor at the Faculty of Industrial Sciences & Technology, Universiti Malaysia Pahang. He has 16 years of research experience in the synthesis and characterization of advanced functional materials. His current research interests cover the application of nanomaterials in the field of energy storage and biosensors.

oxides, and clays.[37] Accordingly, the combination of MOFs with polymer fibers enables the formation of fiber composites with advantages over conventional materials. They offer improved molecular transport through the material and easier access to the active sites of MOFs. These properties make composites attractive for air filtration, biomedical delivery, water treatment, and sensor applications.[37] For example, the limitations of some catalysts are associated with limited diffusion to active sites, and MOF–nanofiber composites can overcome these limitations owing to their open networks and tunable functionality.[38]

Ostermann *et al.* produced the MOF polymer–nanofiber composite from a zeolitic imidazolate framework-8 (ZIF-8) and polyvinylpyrrolidone (PVP) in the electrospinning process.[39] This combination took advantage of both types of material to create a unique class of hierarchical nanostructures that makes the composite structures highly attractive for environmental applications. Efome *et al.* published the first innovative work on developing a nanofiber MOF membrane to separate heavy metals (Pb and Hg) from an aqueous medium.[40]

The removal of HMIs from water by MOFs has been the subject of several excellent reviews. In particular, to the best of our knowledge, no review articles have focused on MOFs–nanofiber composites for removing HMIs. Kobielska *et al.*[41] summarized several research papers covering various areas that remove HMIs from water using MOFs. Yan *et al.*[42] focused on recent advances in MOF materials and MOF membranes to explore their applications for removing Hg ions from water. Chen *et al.*[43] mainly highlighted the recent developments in applying water-stable MOFs and MOF-based materials for the decontamination of HMIs. The most recent review by Li *et al.*[44] focused on the recent advances in using water-stable MOFs to reduce HMIs in water through adsorption and photocatalysis. However, there is no discussion of the substantial removal of HMIs by MOFs–nanofiber composites, or the information provided is not clear and easily accessible. A literature review was performed by scanning the published materials using the Scopus database. The keywords "MOFs, nanofiber, and metal ions" were used as the search keywords. Therefore, for the first time, this review focuses on recent developments of MOFs on nanofibers for the removal of HMIs with many illustrative examples and a thorough investigation of the influencing factors and interaction processes. There are also debates about the challenges and potential of using MOFs in this area.

2. Overview of metal–organic frameworks

Metal organic frameworks consist of diversified metal centers and various organic ligands and have adjustable structures.[45,46] They have attracted significant attention owing to their unique properties and numerous functions.[47] The use of MOFs as self-templates or analogs for producing porous metal oxides by thrombolysis within regulated calcination situations has long been a controversial research topic.[47] Materials have been used in catalytic solutions, either as salts or compounds, to accelerate various chemical processes.[48] MOFs are a novel porous layer material that differ from typical porous materials in terms of the porosity and thermal stability. To date, over 20 000 different MOFs structures have been identified and researched.[49]

Many toxins are released into the atmosphere owing to industry and the growth of production that are seriously harmful to human health. It is, therefore, necessary to implement successful strategies for dealing with these pollutants.[50] They offer great flexibility in construction and are good choices for many different applications.[51] The intrinsic diversity of MOFs enables precise monitoring of the physio-chemical properties of the structures.[50] The poor insulation performance of MOF membranes is usually caused by inconsistent growth at the auxiliary membrane gateway, poor moisture balance, and poor control over porous material pathways.[52]

Metal organic frameworks have a large surface area, a good pore volume configuration, and a wide range of chemical properties, frameworks, and post-synthetic mechanisms that can profoundly alter the chemical structure of the MOF. Thus, MOFs are ideal for various applications owing to these properties. Gas isolation, adsorption, selective catalysis, sensors, and potential drugs carriers are just a few examples .[53] In addition, by adding chemical bonds to linkers, specific MOFs can be further tailored to the desired application. Owing to their versatility, MOFs are effective in various fields, including natural gas and insulation.[54] However, among these purposes, the composition and microstructure of MOFs are not the only factors that should be considered. The specific surface area and the number of material defects can significantly influence their behavior. Coordination modulation can be used to intelligently monitor the material morphology, density, defects, and crystallinity of the MOFs.[55] In addition, the incorporation of unique nanoparticles into MOFs creates a much more stable substance owing to their constant micro-porosity.[56]

2.1 Synthesis of metal–organic frameworks on nanofibers

Natural polymers, such as carbon nanotubes (CNTs), minerals, metal oxides, and multicomponent hybrids are crucial for environmental applications. Depending on the application, porous materials can be processed using various synthetic methods, such as coarse gelling and soft templating.[57] Here, MOF model pyrolysis can be used to develop nanostructured carbon-based products.[58] On the other hand, soft synthesis is based on even more complex physical or chemical associations between the system source and the prototype to guide the specific formation and better regulate the mechanical properties.[57] Weak fabrication is a more active way of fabricating ordered and disordered porous matrices than the other two structure-directing approaches.[57] Amorphous materials are typically produced using the solvothermal process as this is a gentle structure-directing method. MOFs can be used as a pure precursor metal to fabricate various nanoparticles made from MOFs, and the organic components are being used as a carbon source.[57] Based on their final microstructures, MOFs can be made using various synthetic routes, including slow diffusion, hydrothermal (solvothermal), electrochemical

mechanochemical, microwave-assisted heating, and ultrasound methods.[59] MOFs consist of two main components, metal centers and organic linkers. For this reason, their configurations can be tailored to achieve optimal properties for the particular application. Synthesis strategies for the fabrication of MOFs nanofiber materials can be broadly classified as *in situ* MOFs on nanofiber surfaces and synthetic composites from pre-synthesized MOFs.

2.1.1 *In Situ* MOFs on the surfaces of nanofibers. The Küsgens group pioneered the *in situ* synthesis of MOFs on nanofiber substrates.[60] Using the solvothermal method, many kraft pulp fibers and paper sheets were used to help form HKUST-1 MOF, also known as MOF-199.[61] The addition of the fibers to the heated HKUST-1 precursor solution resulted in the production of MOF particles on the substrate. The group observed that pulp fibers with more lignin had a greater HKUST-1 loading. The carboxyl groups on the lignin are similar to the benzene tricarboxylate linker of the MOF, which enables a higher MOF loading. Unfortunately, inconsistent amounts of fiber lignin on the pulp fiber surface resulted in unbalanced coverage. SEM images show that the presence of weakly bound HKUST-1 particles on the fiber surfaces were unstable. In direct solvothermal synthesis, most MOF nucleation occurs in the solvent rather than on the fiber surface, resulting in reactor waste. Consequently, direct solvothermal technology limits the resulting MOF mass loading on the fiber.

Liu *et al.* used electrospun nanofibers made of poly(acrylic acid), poly(vinyl), and SiO_2 in a MOF precursor to increase the loading of the MOFs on the surfaces.[62] The precursor then supported four different MOFs. HKUST-1 and MIL-53(Al) were applied to fiber substrates using a conventional solvothermal method, while ZIF-8 and MIL-88B(Fe) were integrated into a microwave solvothermal synthesis. They achieved minimal MOF growth after one cycle of the solvothermal synthesis, even though functional groups (–OH and –COOH) were presented on their fiber surface. The repetition of the solvothermal synthesis process produced composite samples with the designations HKUST-1-m1, HKUST-1-m2, HKUST-1-m3, and HKUST-1-m4 (Fig. 1a–d). As the growth cycles were repeated, more MOF crystals were formed in the fiber, as shown in the powder X-ray diffraction pattern (PXRD), as shown in Fig. 1e.

In another study, HKUST-1 MOF, also known as Cu-BTC, was synthesized on pretreated anionic electrospun cellulose using a layer-by-layer approach that resulted in a nanoporous material.[63] The anionic pretreatment improved the synthesis of HKUST-1 on the surface of the nanofibers. The carboxymethylated electrospun cellulose was best suited for HKUST-1 functionalization because the HKUST-1 crystals were evenly distributed on the nanofiber surface. The approach described for the surface modification of cellulose for the synthesis of MOF/cellulose materials presented in this work opens up possibilities for MOF synthesis on other cellulose materials, such as nanocrystalline cellulose and micro-fibrillated cellulose.

Ma *et al.*[64] developed a green, aqueous, and template-free synthetic approach for textile-fiber production to produce zirconium MOFs (UiO-708 and MOF-66-NH_2). They found that trifluoroacetic acid (TFA) plays a crucial role as a modulator in synthesizing a consistent growth morphology on a fiber surface. Owing to the direct application of TFA, the fibrous carrier was used exclusively in MOF crystallization and not as an open-flowing solvent suspended powder. Interestingly, most MOF particles were replaced by TFA with other organic acids, such as acetate acid and formic acid, resulting in a non-homogeneous MOF coating on the fiber. The conductive nickel-2,3,6,7,10,11-hexahydroxytriphenylene (Ni-HHTP) and nickel-2,3,6,7,10,11-hexaaminotriphenylene (Ni-HITP) nanosheets on CNFs have been successfully synthesized using interfacial synthesis for the formation of nanofibrillar CNF@ c-MOF (Fig. 2a).[65] With this strategy in mind, we proposed that the fabrication of continuous nucleated c-MOFs nanosheets on CNFs would increase the electrical conductivity of nanocomposites by reducing the grain boundaries and contact resistance, the c-MOFs also increased the flexibility of the nanocomposite.

The second method of growing MOFs on nanofibers is known as biomineralization synthesis. It refers to the process of increasing the mineralization of inorganic materials to make the biomineral shells and the generation of skeletal tissue more robust, thereby providing a solid anchoring surface. For example, two zeolitic imidazole framework (ZIF-8 and ZIF-67) MOFs were grown on electrospun silk nanofibers as a biomacromolecule substrate to produce MOFs–fiber composites.[36]

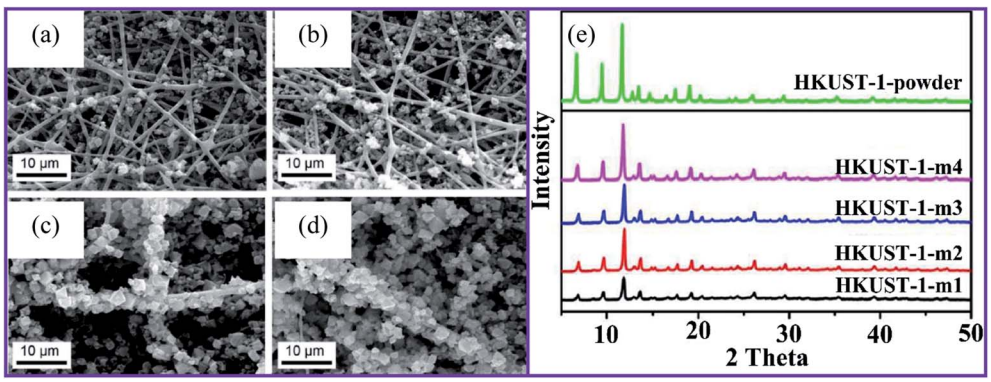

Fig. 1 SEM images of HKUST-1 on nanofibers after (a) one, (b) two, (c) three, and (d) four repetitions of the growth cycles, (e) XRD patterns for the HKUST-1 MOF composites, this figure has been adapted from ref. 62 with permission from American Chemical Society, copyright 2016.

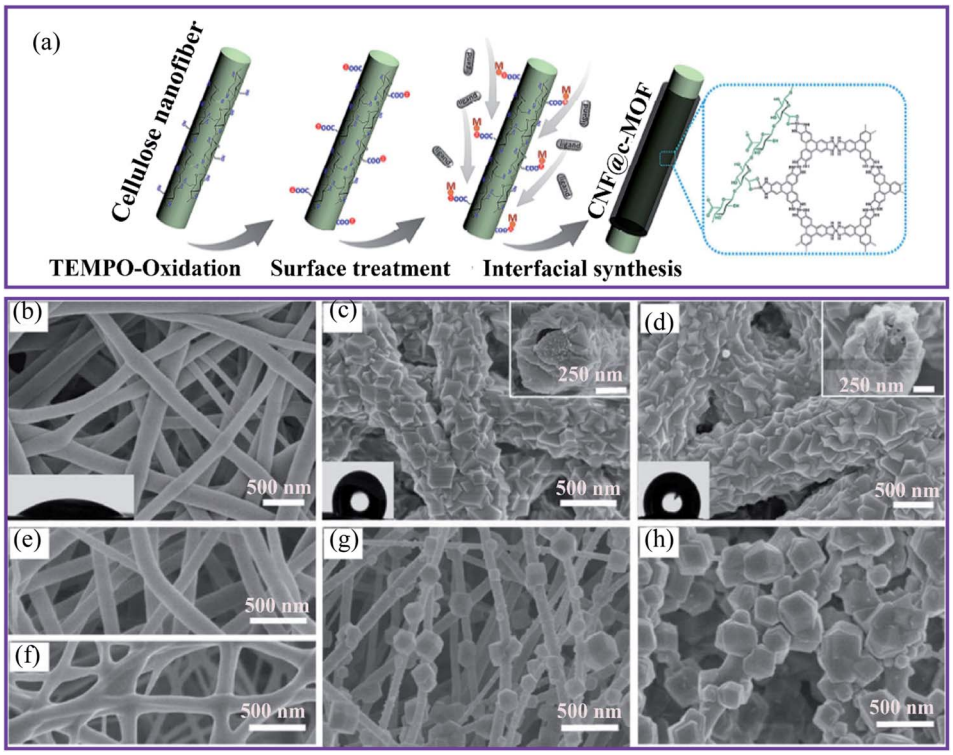

Fig. 2 (a) Schematic diagram of the synthesis of CNF@c-MOF nanofibers.[65] SEM images of (b) the electrospun silk nanofibers, (c) ZIF-8/nanofibers, the inset shows the sectional view from the top, (d) ZIF-67/nanofibers with the sectional view shown in the inset, (e) polyacrylonitrile, (f) polyurethane, (g) PAN@ZIF-8 and (h) PU@ZIF-8 membranes, this figure has been adapted from ref. 36 with permission from the Royal Society of Chemistry, copyright 2018.

The composites were covered using crystalline coatings (Fig. 2b–d) and PXRD was used to verify the structures of the desired ZIFs. In addition, the SEM image recordings of sectional views revealed a core–shell structure. In particular, the MOF layer had a unique intergrown architecture, which indicates the excellent stability of the layer. Furthermore, the authors investigated two synthetic nanofibers, polyacrylonitrile (PAN) and polyurethane. Nonetheless, the manufacture of these synthetic polymer substrates resulted in loosely developed patterns of poorly homogeneous fibers (Fig. 2e–h), underscoring the importance of chemical structures for inducing MOF nucleation and the formation of silk bio-substrates.

The layer-by-layer process (LbL) improves the growth of MOFs on fiber substrates with functional groups, such as COOH and NH_2. For example, Morsali and colleagues investigated an ultrasound-assisted LbL technique for growing CuBTC MOF[66] and zinc terephthalate MOF (MOF-5)[67] on a silk fiber surface. The silk substrates were successively dipped into a metal salt solution, and they were washed using an organic ligand solution to remove any unreacted precursors. In both cases, the sonication increased the LbL growth process and enhanced the homogeneity of the MOF coating on silk fibers. However, this technique hampered the production of MOF–silk composites with a high mass loading and full coverage. The lack or low density of functional groups on the untreated surface of the fiber made it impossible for MOF anchoring events to occur during the LbL process, which probably caused the inadequate coverage.

Another technique was developed to fabricate MOFs–nanofiber composites that directly took advantage of the coordination replication from an inexpensive, insoluble precursor. Fig. 3a shows the method established by Kitagawa and colleagues.[68] The authors succeeded in creating a well-structured MOF architecture $[Al(OH)(ndc)]_n$ by morphological substitution of a shaped sacrificial metal oxide (Al_2O_3), which served both as a metal ion source and as an architecture-controlling agent. As can be seen in Fig. 3b, the field emission scanning electron microscopy (FESEM) image demonstrated that the fibrous architectures were retained even after the conversion of aluminum oxide to aluminum-based $[Al(OH)(ndc)]_n$. Characteristic block crystals with a size of several hundred nanometers were grown on the surface of the aluminum oxide nanofibers. In addition, this method provided 1D nanofibers based on Al–MOF. A simple solution-processed technique was used to make alumina nanofibers for 1-D Al–MOF nanofiber manufacture.

2.1.2 Synthesis of MOF–nanofiber composites from pre-synthesized MOFs. The electrospinning process has emerged as a way of making MOFs–nanofiber composites. Under high voltages, the mixed suspension of MOF nanoparticles and polymers is spun.[69,70] The technique has resulted in the fabrication of polymer substrates that are typically miscible in polar organic solvents, such as dimethylformamide (DMF). Many

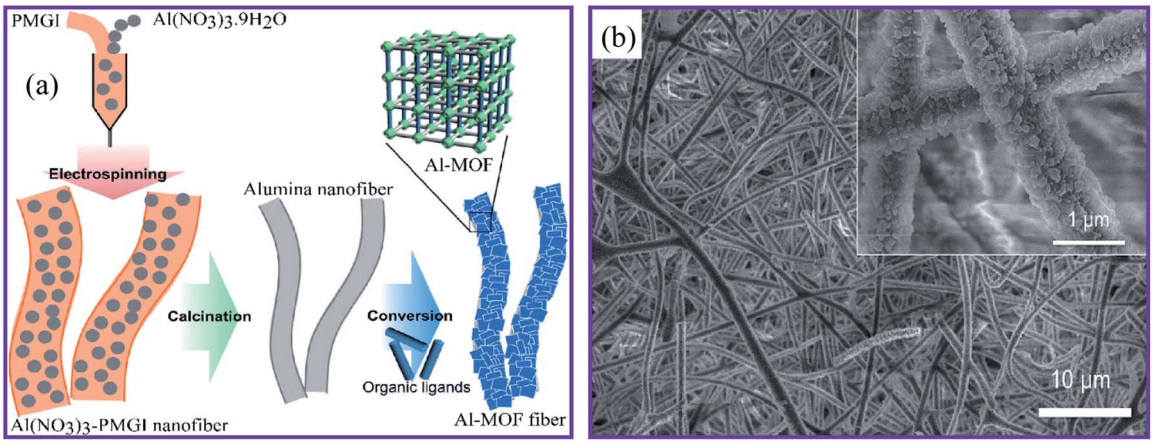

Fig. 3 (a) Schematic presentation of the synthesis of the Al–MOF fibrous architectures. (b) FESEM image of the Al–MOF nanofibers at pH 4.3, this figure has been adapted from ref. 68 with permission from the Chemical Society of Japan, copyright 2014.

polymers, including polystyrene (PS), PAN, PVP, and polyvinylidene fluoride (PVDF), have been used as substrates in electrospinning technology to make MOFs–nanofiber composites. Wang *et al.*[71] demonstrated the generalizability of this manufacturing approach to various polymer substrates, including PAN, PS, and PVP, while supporting doped MOF nanoparticles, as shown in Fig. 4. The technique produced an extremely high MOF mass loading and excellent MOF particle dispersion behavior.

Interestingly, MOF nanoparticles retained their porosity and surface area after post-synthetic deposition on the fiber. They also used various carrier substrates, such as metal mesh or fleece, to reinforce the structure of the MOFs–nanofiber composite and increase its resilience. Although structurally improved, electrospun composites could not be used in other

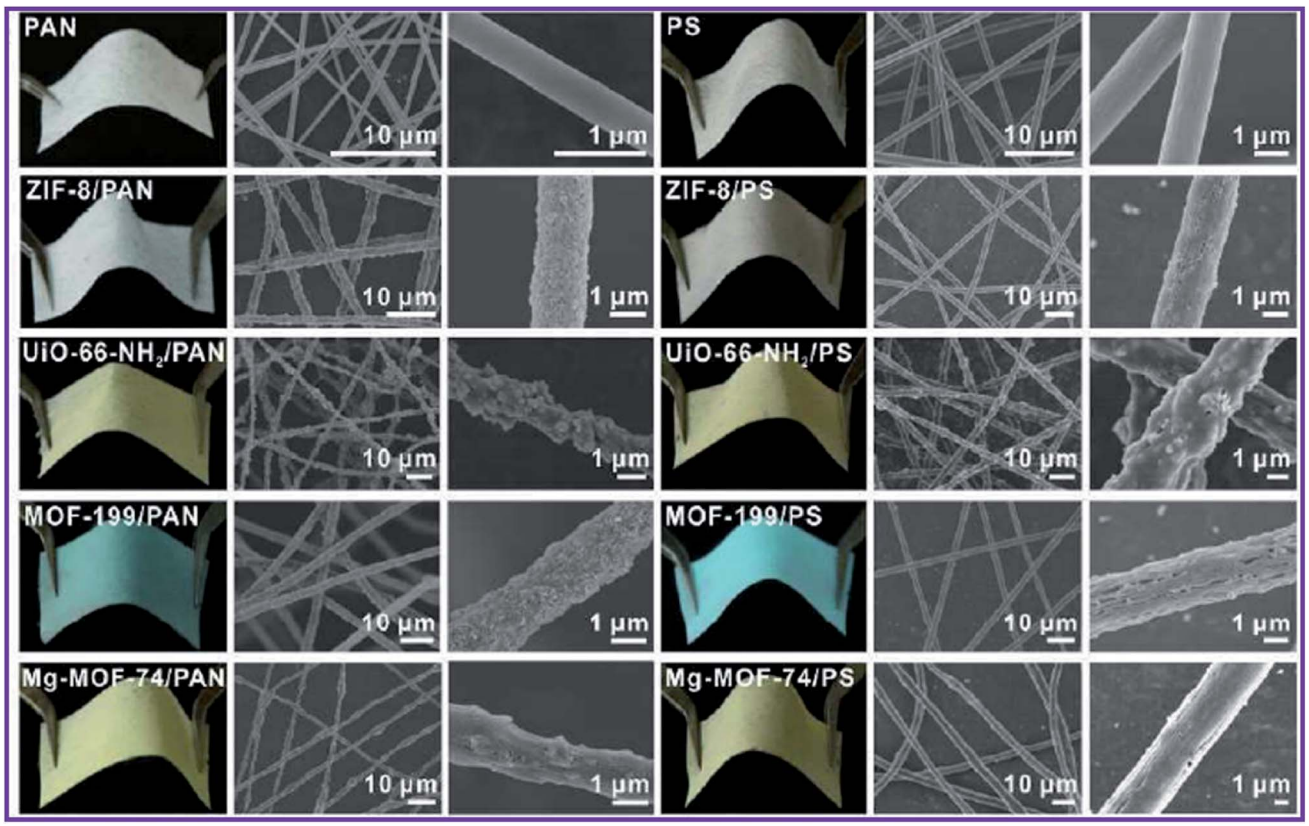

Fig. 4 Photographs and SEM images of MOF–PAN nanofibers and MOF–PS nanofibers composites supported on a piece of fabric, this figure has been adapted from ref. 71 with permission from American Chemical Society, copyright 2016.

media such as DMF owing to the solubility of polymer substrates in these polar solvents.

The electrospinning approach to post-synthetic MOF deposition on fibers was developed by López-Maya *et al.*[72] They developed a method by which MOF nanoparticles can be inserted into silk nanofibers, a novel approach for doping nanofibers during electrospinning. The suspension of zirconium 1,4-dicarboxybenzene MOF (UiO-66 MOF), which is an acronym for Universiteteti (Oslo),[73] was scattered over the silk nanofibers during the electrospinning process. In the empty silk nanofiber substrate, the incorporated MOF nanoparticles created a UiO-66–nanofiber composite. Although this method provides significant mass loading of the MOF loading in the composite, the low interactions between the MOF and the fiber led to an unstable composite. The leaching of the functional MOF nanoparticle limits the economic viability of this manufacturing process.

The microwave heating approach was used by Jamshidifard *et al.* to create UiO-66-NH_2 MOF. The UiO-66-NH_2 MOF was then electrospun onto the surface of the PAN-chitosan nanofibers to produce the UiO-66-NH_2–PAN-chitosan nanofiber composite. The XRD patterns show that the UiO-66-NH_2 MOF was effectively integrated into the PAN-chitosan nanofibers, and the electrospinning process did not affect the crystal structure UiO-66-NH_2 MOF.[74] There was no significant change in the observed peak spectrum for UiO-66-NH_2 and PAN-chitosan in the Fourier transform infrared spectroscopy (FTIR) spectra, indicating the combination of UiO-66-NH_2 and PAN-chitosan did not influence the chemical structure of UiO-66-NH_2 MOF.

2.2 MOFs–nanofiber composite characteristics

Porous morphologies exist in many materials, varying from carbon-based to metal-based materials (oxides, carbides, chalcogenides, and phosphides).[75–77] Porous materials contain voids that are interconnected to form channels that positively affect the design of materials with attractive properties. MOFs have a high porosity that can reach up to 90% of the free volume, and possess large internal surface areas, approaching 7000 $m^2\ g^{-1}$, and concentrated metal sites.[78,79] Therefore, MOFs have shown significant promise in various applications, including sensing, gas separation, storage, catalysis, and electrical and optical devices.[80,81] Owing to the high porosity of the MOF structure, the choice of supporting substrate can influence the flexibility, robustness, and processability of the MOF-based composite. Fiber materials are among the least expensive and most abundant substrates for MOF-based composites. Tuning the polymer composition, fiber thickness, permeability, porosity, and flexural rigidity allows us to target perfect characteristics for different applications. For example, the diameter and porous structure of the PAN-chitosan–UiO-66-NH_2 nanofiber composite can be effectively adjusted by changing the loading ratio of the UiO-66-NH_2 MOF.[74] Fig. 5 shows scanning electron microscopy (SEM) images of nanofiber composites with different UiO-66-NH_2 ratios. For PAN-chitosan nanofibers, smooth nanofibers with an average diameter of 235 nm were produced. The SEM images of 5 and 10 wt% of UiO-66-NH_2 MOF-loaded nanofibers showed a well-defined shape with average diameters of 275 and 345 nm, respectively.

Compared to pure PAN-chitosan nanofibers, the fiber diameter of PAN-chitosan increases by 5 and 10 wt% UiO-66 MOF, enhancing the solution viscosity. MOF crystals were discovered on the surface of PAN-chitosan–UiO-66-NH_2 nanofibers with 15 wt% MOF, the behavior of which is attributed to the dispersion of the MOF crystals, both in the inner pores of the nanofibers and the surface of the nanofibers. The aggregation of UiO-66-NH_2 MOF crystals at higher MOF concentrations (15 wt%) can lead to the formation of MOF crystals with larger sizes than those of the PAN-chitosan nanofiber diameter and, as a result, exposed UiO-66-NH_2 MOF crystals on the surface of the nanofibers. The porosity of the nanofibrous membranes containing 0, 5, 10, and 15 wt% of UiO-66-NH_2 MOF were determined to be 87, 82, 78, and 71%, respectively.

3. HMIs removal *via* MOF-based nanofibers materials

Controlling HMIs in water is challenging owing to their bioavailability and non-degradability. Owing to their longevity, HMIs are more important than other pollutants, such as organic compounds. Researchers have studied various materials and methods of removing HMIs for many years.

Adsorption is popular owing to its adaptability, simplicity, cost-effectiveness, and easy replication.[82,83] Activated carbons, molecular sieves, chitosan, polymers, and biomass materials are examples of materials with a traditional adsorption capacity.[84] However, they have a low scalability, sensitivity, and, above all, adsorptive capacity. This creates the opportunity to develop innovative adsorbents with a good specificity and adsorption potential for environmental and water detoxification applications.

3.1 Removal of bivalent heavy metal ions

Peng *et al.*[85] reported the fabrication of ZIF-8 MOF on electrospun PAN nanofiber membranes (ZIF-8–PAN nanofibers) using an *in situ* growth technique that includes electrospinning and hot-pressing (Fig. 6a). The ZIF-8–PAN nanofiber membrane exhibited a high water flux of 12 000 L $m^{-2}\ h^{-1}$ with a high filtration efficiency of 96.5% for Cu(II) removal. In addition, the ZIF-8–PAN nanofibers showed a strong dynamic adsorption and remarkable filtering efficiency (96.5%). In addition, the removal rate of Cu(II) in 4 min reached 34.1% using a combination of adsorption and electrochemistry. The adsorption results demonstrated that the adsorption kinetics of Cu(II) ions on ZIF-8–PAN nanofibers agree well with the second-order model. The maximum capacity was 225.62 mg g^{-1}. Furthermore, the excellent durability of the ZIF-8/PAN nanofiber makes it a suitable membrane for real water treatment applications. The investigations showed that the high specific surface area, abundant active sites of the ZIF-8 nanoparticles, and the reduced equivalent apparent pore size of the membrane by hot

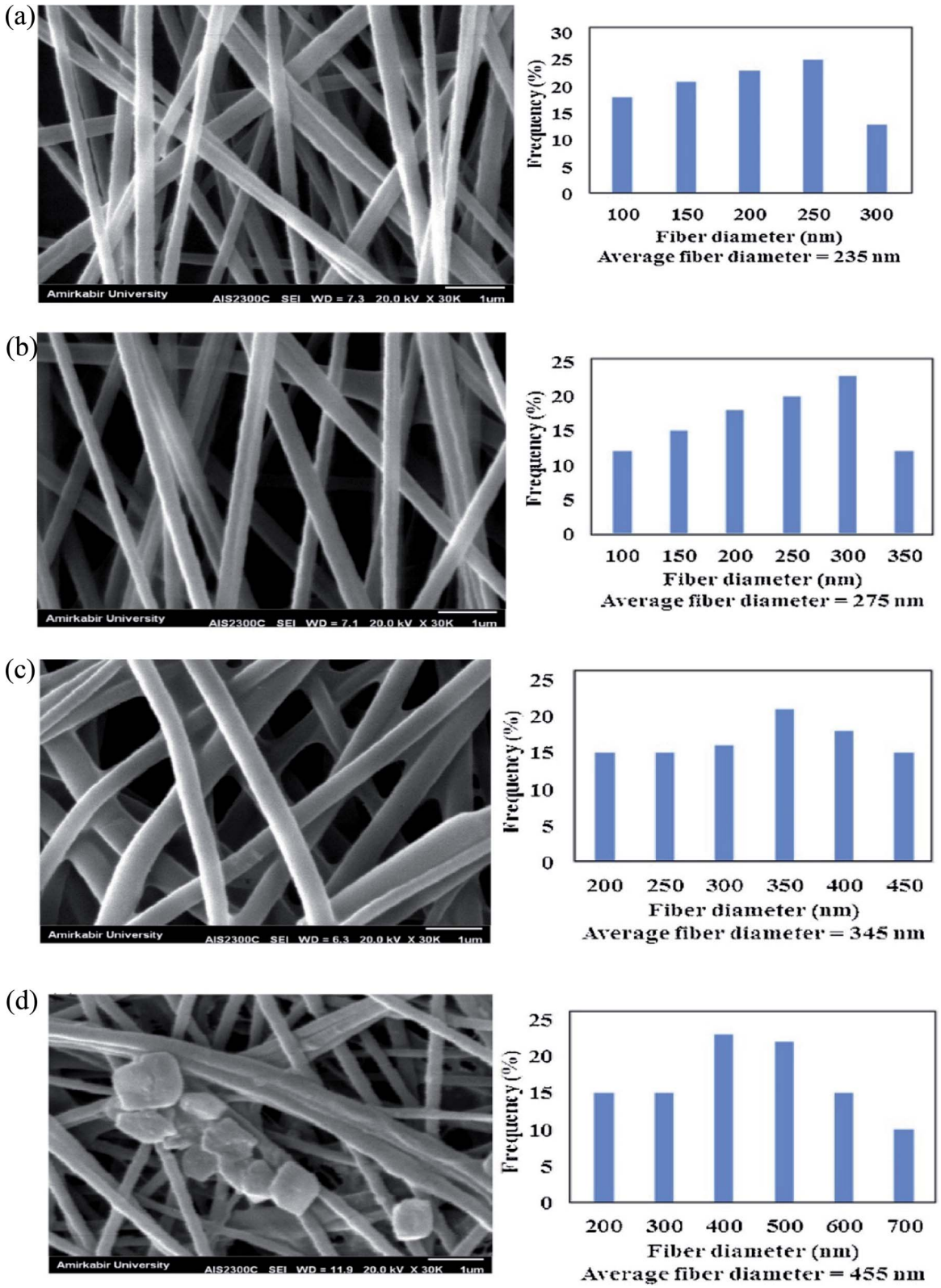

Fig. 5 SEM images and fiber diameter distribution of (a) PAN-chitosan nanofiber and nanofibers containing (b) 5 wt% UiO66-NH_2 MOF, (c) 10 wt% UiO66-NH_2 MOF and (d) 15 wt% UiO66-NH_2 MOF, this figure has been adapted from ref. 74 with permission from Elsevier, copyright 2019.

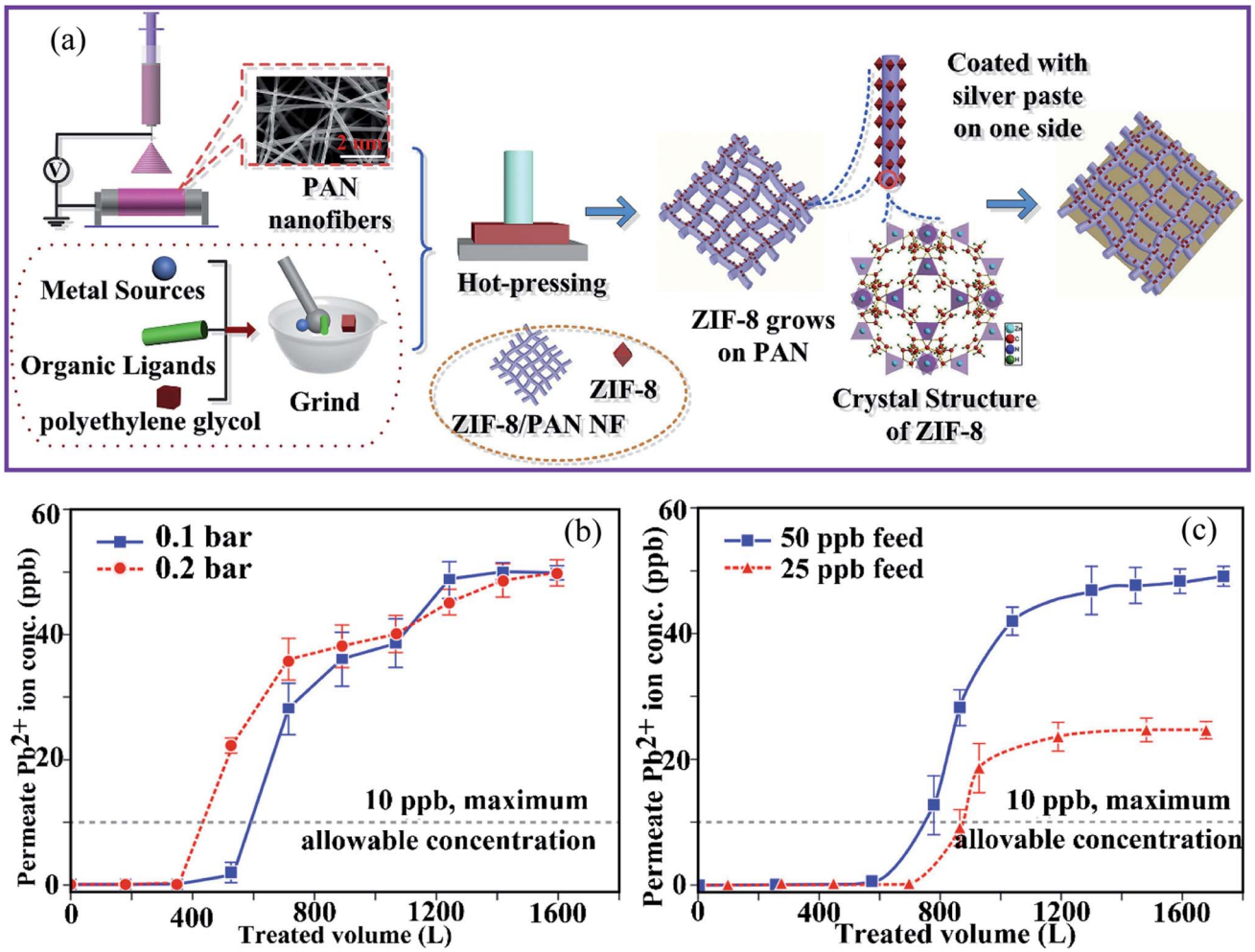

Fig. 6 (a) Schematic diagram of the preparation of ZIF-8–PAN–Ag, this figure has been adapted from ref. 85 with permission from Elsevier, copyright 2020. Effects of (b) changes in TMP relative to the permeate quality and (c) initial lead ion concentration in the feed on the permeate lead ion concentration (TMP = 0.1 bar, flux = 348.9 kg m^{-2} h^{-1} and TMP = 0.2 bar, flux = 693.6 kg m^{-2} h^{-1}, membrane thickness = 560 μm, feed concentration = 41.7 × 10^{-3} mg L^{-1}, and ambient temperature), this figure has been adapted from ref. 86 with permission from Elsevier, copyright 2019.

pressing contributed to the superior filtration performance of ZIF-8–PAN for Cu(II) ions.

Similarly, Efome *et al.*[86] reported on the fabrication of PAN–MOF-808 nanofibers using co-electrospinning of MOF-808 and the PAN polymer. These were then used as adsorption filters to remove Pb(II) ions from an aqueous medium to investigate the effect of various process parameters, such as transmembrane pressure (TMP), concentration, and membrane thickness. It was found that a decrease in TMP and in the initial feed concentration, and an increase in the membrane thickness have the greatest influence on increasing the treated feed volume (Fig. 6b and c). On the other hand, the moderate adsorption capacity (18–37%) was attributed to the existence of other coexisting ions in water (*e.g.*, Na^+, Mg^{2+}, and Ca^{2+}), as well as the influence of their electronegativity and the ionic radius of Pb(II).

The UiO-66-NH_2 MOF crystal was developed and integrated by Jamshidifard *et al.*[74] into PAN-chitosan nanofiber membranes to produce the UiO-66-NH_2–PAN-chitosan composite. The synthesized MOFs and nanofibers were used to remove the Pb(II) and Cd(II) ions through adsorption and membrane filtration. The UiO-66-NH_2 MOF crystals were observed on the surface of the nanofiber, and this behavior can be attributed to the distribution of the MOF crystals in the inner pores and surface of the nanofibers. The capacity for metal ion sorption was improved by increasing the initial Pb(II) and Cd(II) levels and therefore increasing the numbers of metal ions available for chelation with the adsorbent binding sites. Saturation at a high concentration of the active metal ion centers of the PAN-chitosan–UiO-66-NH_2 nanofiber adsorbent resulted in a slight change in the Pb(II) and Cd(II) adsorbent capacity for aqueous solutions. In addition, the slight decrease in the adsorptive capacity of Pb(II) and Cd(II) ions using the composite nanofiber adsorbent after five regeneration cycles demonstrated the excellent reusability of the adsorbent for practical applications. The sorption data could be well fitted using the Redlich–Peterson isotherm model, indicating that the monolayer adsorption of Pb(II) and Cd(II) ions was the

predominant reaction. In addition, the high water flux and good removal of ions within 18 h of the filtration time showed the high potential of the UiO-66-NH_2–PAN-chitosan membrane for the removal of metal ions from aqueous solutions.

The MOF composite membrane was fabricated by co-electrospinning of the Zr-based MOF-808 ($[Zr_6O_4(OH)_4(COOH)_6(BTC)_2]$) and hydrophilic PAN nanofibers after using different routes to activate MOF-808 to increase the adsorption capacity (Fig. 7a) for the removal of Cd(II) and Zn(II) ions from an aqueous solution.[87] The composite membrane containing 20 wt% MOF was used for the removal of Cd(II) and Zn(II) ions from an aqueous solution (Fig. 7b and c). Owing to the incorporation of the MOF particles, the PAN–MOF-808 composite had a significantly larger fiber diameter than that of the PAN, with pore diameters ranging from 0.5–1 μm, which contributed to an increase in the surface roughness. The highest adsorptive capacities of Cd(II) and Zn(II) were 225.05 and 287.06 mg g^{-1}, respectively.

The MOF-808–PAN membrane exhibited a high water flux of 348 L m^2 h^{-1} for Cd(II) owing to the high adsorptive capacity of the MOF and its ability to be accessed in the enclosed form. In addition, the Langmuir adsorption isotherm model is more suitable than the Freundlich and Temkin models in terms of consistent experimental data. Thus, the highest adsorptive capacities found for Cd(II) and Zn(II) were 225.05 and 287.06 mg g^{-1}, respectively. The MOF-808–PAN membrane has been suggested as a suitable membrane for water treatment because of its excellent separation performance, reusability, and superior water stability.

Hou *et al.*[88] used a simple *in situ* growth technique to generate a zeolitic imidazolate framework-67 (ZIF-67) MOF that was fused onto the surface of electrospun nanofibers made from 2-methylimidazole–cellulose acetate (MIM–CA) (Fig. 7c). The ZIF-67 particles adhere to the CA fibers in an orderly manner, similar to the structure of a pearl chain. The unique

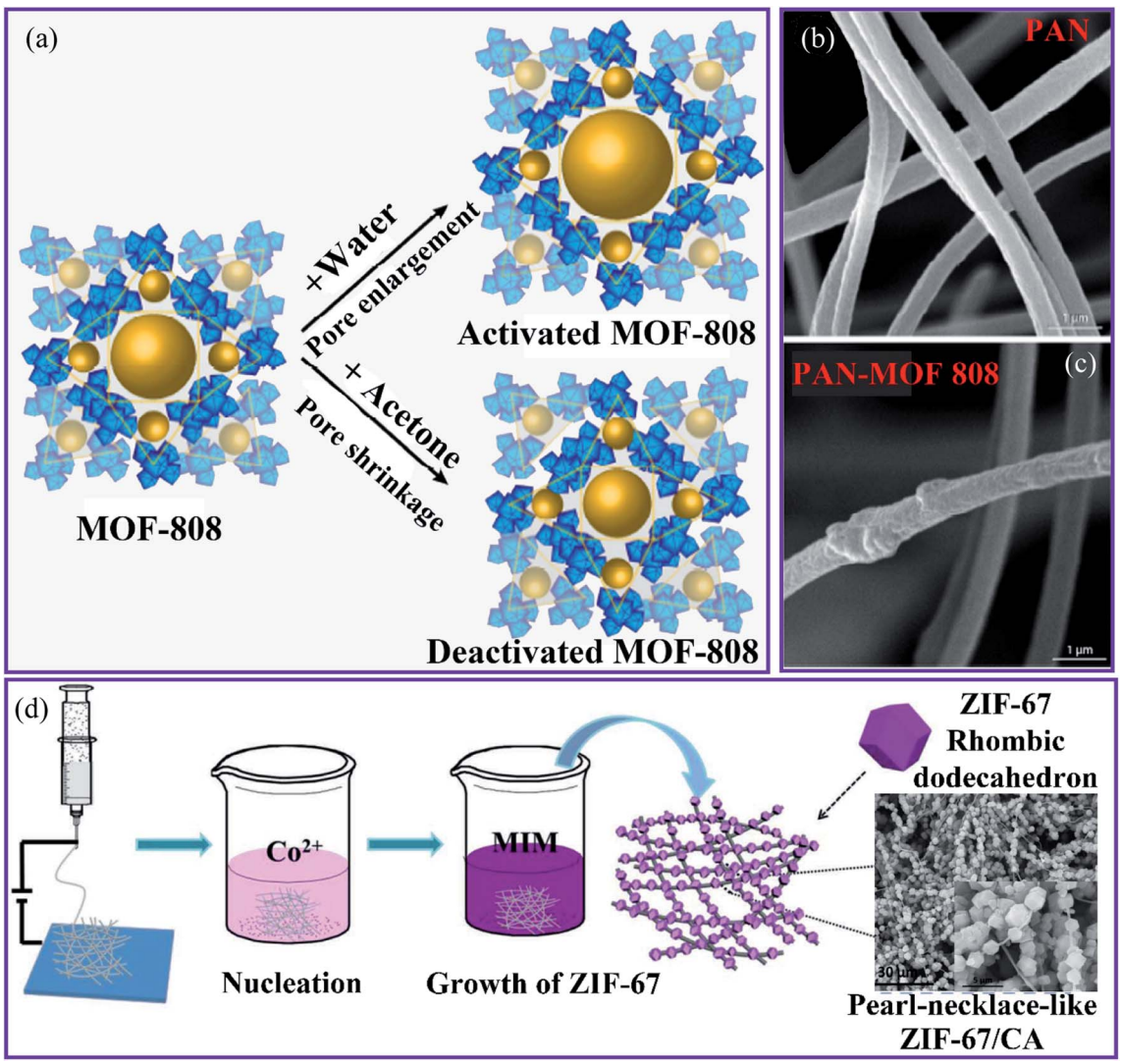

Fig. 7 (a) The activation routes of MOF-808. SEM images of the nanofibrous membranes of (b) PAN and (c) PAN–MOF-808, this figure has been adapted from ref. 71 and 87 with permission from American Chemical Society, copyright 2018. (d) Schematic representation of the synthesis of the ZIF-67–CA composite, this figure has been adapted from ref. 88 with permission from Willey Online Library, copyright 2018.

composite was used to remove Cu(II) from wastewater. The composite had a high Cu(II) adsorption capacity of 18.9 mg g^{-1}, and the adsorption results were in good agreement with the pseudo-second-order kinetics. This was attributed to the increased specific surface area and the adsorption sites on the adsorbent provided by the pearl-necklace-like structure, which prevented the agglomeration of ZIF-67 and promoted contact between the composite and Cu(II) ions. Using an ultrasound-assisted method, Mahmoodi *et al.* synthesized ZIF-67 crystals that grew and were stabilized on the surface of a magnetic eggshell membrane (Fe_3O_4@ESM) to produce the ZIF-67@Fe_3O_4@ESM composite.[89] Owing to the large surface area (1263.9 m^2 g^{-1}), the composite has a faster absorption rate and a higher performance for removing Cu(II) ions from wastewater. The results indicated that the composite had a maximum adsorption capacity of 344.82 mg g^{-1}. Kinetic and isotherm results indicated that the adsorption process followed the pseudo-second-order model using the Langmuir adsorption isotherm model.

Shooto *et al.*[90] described an electrospinning method for producing PVA–Co-MOF sorbents by combining novel PVA nanofibers with a cobalt metal–organic framework. SEM images showed that homogeneous, bead-free nanofibers were developed. The FTIR spectra showed changes in certain functional group positions, suggesting cobalt metal–organic frameworks were implanted into the interconnected nanofibers. The ability of these novel PVA–Co-MOF nanofibers to remove Pb(II) ions from the solution was investigated. The sorption of Pb(II) ions on integrated nanofibers (PVA-Co-MO) was twice as high as that of pure PVA nanofibers. Moreover, kinetic studies revealed that Pb(II) ion absorption by nanofibers at low temperatures is favored and is dominated by the physisorption process. Pb(II) ion adsorption processes have also been observed using pseudo-second-order model kinetics and the Langmuir adsorption isotherm model.

Using a simple *in situ* loading technique, a ZIF-8 hybrid nanofiber film was effectively fabricated on a polymeric substrate material.[91] A hydrolysis duration of 1 h, a two-cut film, and 0.3% by weight of poly(4-styrenesufonate sodium) (PSS) were identified as optimal conditions. The film prepared under optimal conditions was used to extract the Pb(II) from water, and a high removal efficiency of 99.5% was demonstrated. In addition, compared to the pure PAN film, the removal capacity increased up to three times, and a high permeation flow of 180 L m^2 h^{-1} psi was observed. The process of the adsorption isotherm followed the Langmuir model. Other heavy metals, including Cr(II), Hg(II), Cu(II), and Cd(II), were examined for removal from water using the hybrid film, and the film still exhibited a high removal efficiency. This improvement can be attributed to the unique properties of microporous ZIF-8 as active sites for Pb(II) adsorption with a high surface area of electrospun PAN.

3.2 Removal of variable-valence heavy metals ions

Ashour *et al.* described the production of a hybrid nanocomposite consisting of MIL-100(Fe) MOF immobilized in bacterial cellulose (BC) nanofibers, as shown in Fig. 8a.[92] The resulting nanocomposite reveals a good, mechanically robust, flexible, and ultralight structure. However, small MIL-100(Fe)

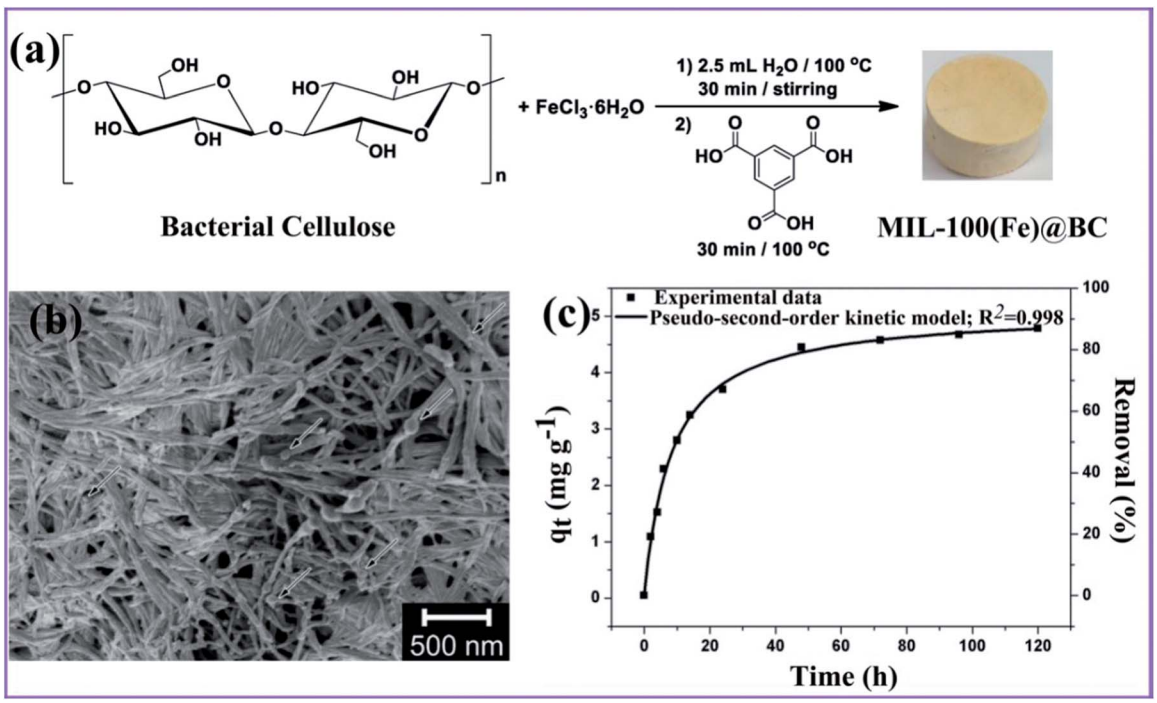

Fig. 8 (a) General approach for synthesizing the MIL-100(Fe)@BC nanocomposite. (b) SEM image of the hybrid MIL-100(Fe)@BC nanocomposite. (c) Adsorption capacity *versus* time, and the nonlinear pseudo-second-order fitting for As(III), this figure has been adapted from ref. 92 with permission from MDPI, copyright 2020.

particles were found in a consistent pattern on the surface of the BC nanofibers (Fig. 8b), and these remained stable enough to form the nanocomposite. The nanocomposite MIL-100(Fe)@BC was used to remove As(III) from an aqueous solution and reached an adsorption capacity of 4.81 mg g^{-1} with a removal efficiency of 85% after 72 h (Fig. 8c). Furthermore, the pseudo-second-order nonlinear fit can accurately represent the adsorption process. This suggests that the BC had no effect on the accessibility of the MIL-100(Fe) pores and that the majority of MIL-100(Fe) particles were active in the chemical process of the adsorption of As(III) onto the MIL-100(Fe)@BC nanocomposite through surface complexation.

Wang *et al.*[93] produced a ZIF-8–PAN nanofiber composite using *in situ* hydrothermal treatment. SEM images reveal that the ZIF-8 nanocrystals grow well in the PAN nanofibers (Fig. 9a and b). The accompanying transmission electron microscopy (TEM) images (Fig. 9c and d) show that the ZIF-8 nanocrystals develop on the surface and inside the PAN fibers. Interestingly, the enlarged TEM image (Fig. 9d) indicates that the mesoporous structures are created during the reaction by PVP etching. The presence of a type IV hysteresis loop in the N_2 adsorption/desorption patterns supports this mesoporous property (Fig. 9e). Owing to their porous architectures, the ZIF-8–PAN filter displayed a significant U(VI) (530.3 mg g^{-1} at pH = 3.0). The adsorption process largely corresponds to the pseudo-second-order model and is mainly chemical adsorption. Furthermore, the results show that the Langmuir model fits the experimental data better than the Freundlich model, confirming that it is a monolayer adsorption process. The ZIF-8–PAN composite exhibited a high U(VI) adsorption capacity of 530.3 mg g^{-1} at pH 3 by taking advantage of its porous properties.

Cr(VI) ions were effectively removed from the aqueous solution at an initial concentration of 50 mg L^{-1} metal ions by the adsorption and membrane filtration processes using the UiO 66-NH_2–PAN-chitosan nanofiber composite.[74] Fig. 9f shows that the capacity of Cr(VI) reached the highest value at pH 3. The electrostatic attraction of the positive charge (protonated amino and carbonated adsorbent groups with a lower pH) of the nanofibers and the negative charge $HCrO_4^-$ can be achieved through the use of PAN-chitosan–UiO-66-NH_2 nanofibers at a maximum Cr(VI) absorption.[95] In comparison, a decrease in the charge density at higher pH values of nanofibers led to a decrease in the effectiveness of the Cr(VI) ion adsorption. Li *et al.*[94] have prepared a zeolitic frame-67 (ZIF-67) MOF modified

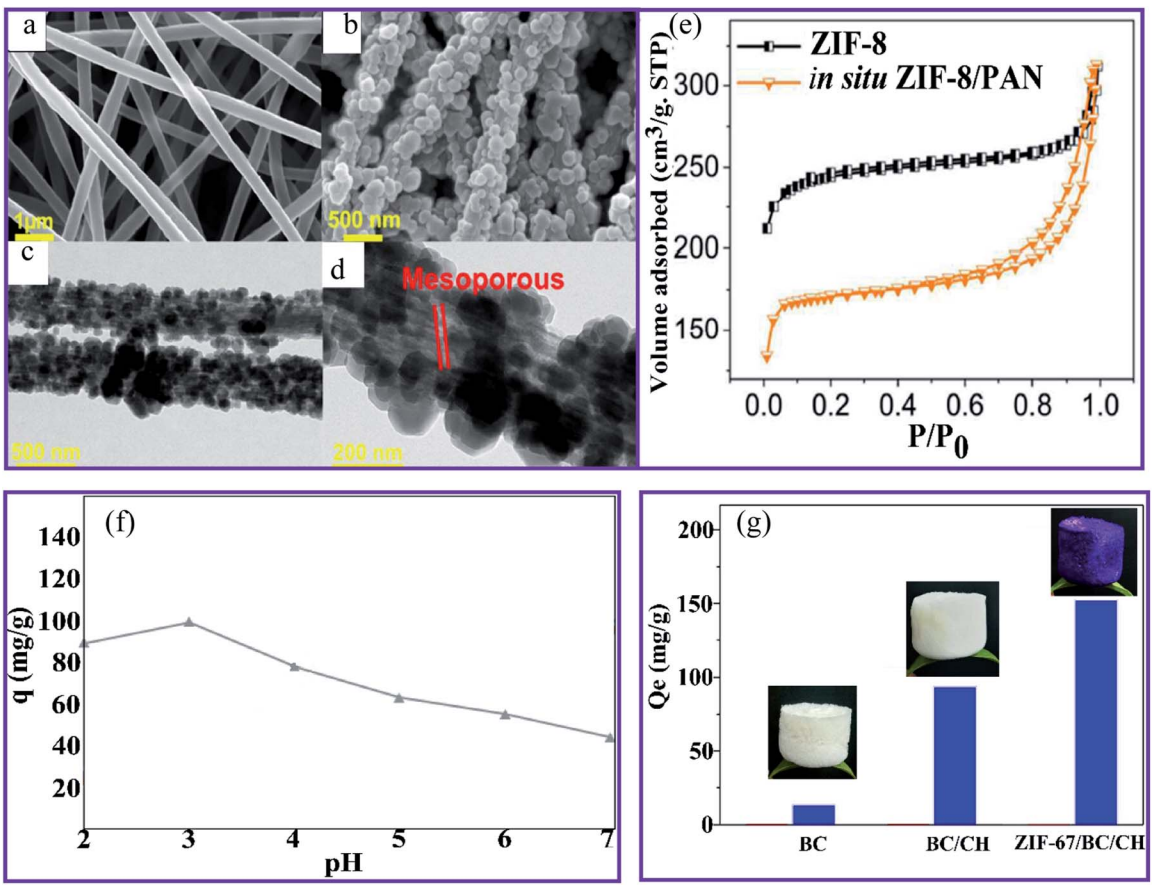

Fig. 9 SEM images of (a) the PAN nanofibers and (b) the ZIF-8–PAN composite. (c) and (d) TEM images of the ZIF-8–PAN composite. (e) N_2 adsorption/desorption measurements of ZIF-8 and the ZIF-8–PAN composite, this figure has been adapted from ref. 93 with permission from American Chemical Society, copyright 2018. (f) The effect of pH on the Cr(VI) ions sorption using PAN-chitosan–UiO-66-NH_2 nanofibers, this figure has been adapted from ref. 74 with permission from Elsevier, copyright 2019. (g) The adsorption capacity of BC, BC–CH, and ZIF-67–BC–CH aerogels for Cr(VI) ions, this figure has been adapted from ref. 71 and 94 with permission from Elsevier, copyright 2020.

Table 1 Summary of the key findings for the removal of HMIs by MOF/nanofiber composites

MOFs–nanofiber composite	Adsorption capacity (mg g^{-1})	Metal ion	Equilibrium time	pH	Adsorbent dose (g L^{-1})	Isotherm/kinetic	Removal (%)	Ref.
ZIF-8–PAN NF	225.62	Cu(II)	600 min	—	—	Pseudo-second-order	97.75	85
MOF-808–PAN	48.67	Pb(II)	—		—	—	47	86
Zr-MOF-808–PAN	225.05	Cd(II)	10 min	4.5	—	Langmuir, pseudo-second-order	~55	87
	287.06	Zn(II)					~60	
ZIF-67–MIM/CA	14.5	Cr(VI)	24 h	6.5	—	Pseudo-second-order	~88	88
ZIF-67@Fe_3O_4@ESM	344.82	Cu(II)	150 min	5	0.006	Langmuir, pseudo-first order	93	89
Co-MOF–PVA	55.23667	Pb(II)	30 min	5.03	—	Langmuir	59.41	90
ZIF-8–PAN	74.1	Pb(II)	3 h	—	—	Langmuir	99.4	91
MIL-100(Fe)@BC	4.81	As(III)	72 h		—	Pseudo-second-order	85	92
In situ ZIF-8/PAN	530.3	U(VI)	60 min	3	—	Langmuir, pseudo-second-order	85	93
ZIF-67–(BC/CH)	200.6	Cu(II)	24 h	6	—	Pseudo-second-order	~96	94
	152.1	Cr(VI)					~93	
UiO-66-NH_2–PVDF/chitosan	602.3	Cr(VI)	25 min	5.5	0.5	Redlich–Peterson/pseudo-second-order	—	96
ZIF-8–PVDF/chitosan	569.3							
UiO-66–poly(arylene sulfide sulfone)	89.12	Cr(VI)	100 min	3.5	—	Pseudo-second-order	—	95
ZIF-67–ANF	250.95	Cu(II)	25 h	6.0	—	Pseudo-second-order	—	97
	183.29	Cr(VI)						

by a simple technique involving physical mixing, *in situ* synthesis, and lyophilization in a cellulose–chitosan (BC–CH) composite aerogel. The water stability of the CH aerogel was improved by using BC nanofibers instead of using chemical linking agents. The loading rate of ZIF-67 was 46.1%, and the Brunauer–Emmett–Teller (BET) specific surface area of the ZIF-67–BC–CH aerogel was 268.7 m^2 g^{-1}, which was considerably higher than that of the BC–CH aerogel area (8.4 m^2 g^{-1}). The aerogel ZIF-67–BC–CH was used to remove the Cr(VI) ions from an aqueous solution with an adsorption capacity of 152.1 mg g^{-1}, corresponding to a higher adsorption capacity than that of the BC and BC–CH aerogel, as observed in Fig. 9g. In addition, the adsorption process fits well with the pseudo-second-order kinetic model, suggesting that chemical adsorption was involved in the overall adsorption process. Coordination, ion exchange, and electrostatic interactions were all involved in the adsorption process of the ZIF-67–BC–CH aerogels. The Cr(VI) ions could be physically adsorbed onto the aerogel *via* electrostatic attraction, and they could coordinate with the pyridinic N of ZIF-67. The ion exchange also took place between the Cr(VI) ions and the hydroxyl linked to the uncoordinated Co(II) of the ZIF-67 crystals.

In another study on the removal of Cr(VI) ions, Pishnamazi *et al.* integrated PVDF nanofibers into UiO-66 NH_2 and ZIF-8 MOF nanoparticles.[96] Then, the PVDF nanofibers were coated with chitosan nanofibers to produce PVDF-chitosan nanofibers. The incorporation of ZIF-8 decreased the hydrophilicity of PVDF and PVDF-chitosan nanofiber membranes. The performance of the ultrafiltration membrane technology for the recovery of Cr(VI) ions was investigated. Interestingly, the highest water flow observed was 470 L m^{-2} h^{-1}, and the efficiency reached 95.6% when a PVDF-chitosan nanofiber membrane with 20 wt% of UiO-66-NH_2 was used.

The maximum sorption capacities of Cr(VI) were determined and found to be 602.3 mg g^{-1}. The pseudo-second-order kinetic model accurately explained the kinetic data for the Cr(VI) sorption. Furthermore, the Redlich–Peterson isotherm model fits the equilibrium data better than the Freundlich and Langmuir isotherm models. The results revealed that the Cr(VI) sorption took place at the synthesized nanofibers' homogeneous and heterogeneous sorption sites. However, sorption of Cr(VI) was the most prominent in the nanofiber monolayer. Wei *et al.*[95] investigated the use of the UiO-66–poly(arylene sulfide sulfone) nanofiber membrane for treating Cr(VI) ions. The nanofibrous membrane exposed a high specific surface area and hydrophobicity structure with a high removal efficiency of 98.44% and a flux of 636 L m^{-2} h^{-1}. Interestingly, this membrane maintained an excellent stable morphology and good removal performance for a range of pollutants after storage in a corrosive and harsh solution, indicating that it could be widely used in complicated wastewater treatment, particularly in hostile conditions. The key results for the removal of HMIs by MOF–nanofiber composites are summarized in Table 1.

3.3 Removal mechanism and kinetics

The effective removal by MOFs can be attributed to the large specific area and functional groups of nanofibers and MOFs

such as carboxylic, amine, hydroxyl, and oxygen for chelation with metal ions resulting in the higher potential adsorbent towards metal ions sorption. Based on the type of interaction between the MOFs and HMIs, the adsorption can be divided into physical and chemical adsorption, as depicted in Fig. 10a. Physical adsorption is known as adsorptive adsorption, in which chemical adsorption is known as reactive adsorption.[98] A typical experimental method used to investigate the possible mechanism is to study the adsorption isotherm of the MOFs-based nanofiber structures.

The Langmuir and Freundlich models often fit the adsorption equilibrium data. The Langmuir model is suitable for the sorption process on homogeneous surfaces, and the Freundlich model is suitable for the sorption process on heterogeneous surfaces.[99,100] Langmuir adsorption is a form of chemical adsorption that is more stable and has a greater capacity than basic physical adsorption.

Adsorption kinetics are a powerful method used to study the adsorption mechanism between MOFs-based nanofibers and HMIs. Almost all adsorption kinetics are better matched with the pseudo-second-order model, as evidenced by the better correlation coefficients compared to the pseudo-first-order model.[89,90,93] In a study by Peng *et al.*,[85] the adsorption data of ZIF-8–PAN NF for Cu(II) were adapted to a pseudo-second-order model ($R^2 = 0.967$). The agreement of the kinetic data with this kinetic model suggests that the adsorption of HMIs on MOFs in aqueous solutions can be controlled by chemical adsorption. ZIF-8 nanoparticles adsorbed Cu(II) in wastewater by the adsorption process, as shown in Fig. 10b. The adsorption process proceeds as follows, first, ion diffusion occurs through different Cu(II) concentrations on either side of the ZIF-8–PAN nanofiltration membrane. Second, heavy metal ions coordinate to the pyridinic N in dimethylimidazole. The metal source and the ligand of ZIF-8 have different capacities for the uptake and loss of electrons, which ultimately leads to a bias in the electron cloud in the direction of the ligand. Thus, it contributed to a more ideal interaction between the hydrogen bond on the N atom and Cu(II). Third, the open metal zinc site in ZIF-8 enables ion exchange between the zinc and copper ions. The pH of the heavy metal ion solution is less than 9.3, indicating that no electrostatic adsorption occurs during the Cu(II) degradation process by ZIF-8–PAN NF.

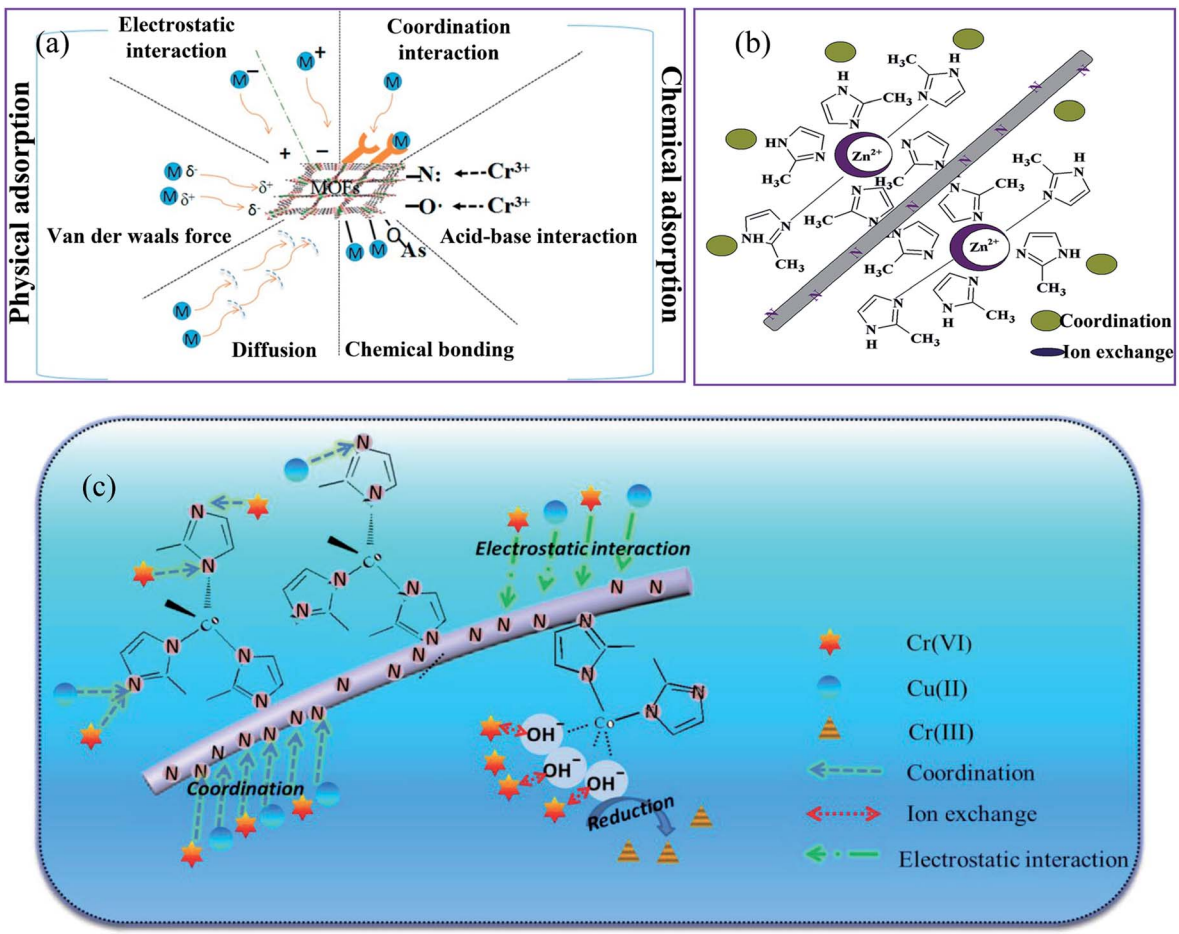

Fig. 10 Schematic diagrams of the possible mechanisms for (a) adsorptive removal of HMIs by MOFs, this figure has been adapted from ref. 98 with permission from Elsevier, copyright 2018, (b) adsorption mechanism for Cu(II) on the ZIF-8–PAN surface, this figure has been adapted from ref. 85 with permission from Elsevier, copyright 2020, and (c) adsorption mechanism for Cr(VI) on the ZIF-67–MIM/CA surface, this figure has been adapted from ref. 88 with permission from Willey Online Library, copyright 2018.

The ZIF-67–MIM/CA composite was used to remove Cr(VI) ions through the interactions shown in Fig. 10c,[88] including physical adsorption driven by the concentration gradient and electrostatic attraction, the coordination between the metal ions and the pyridinic N of 2-methylimidazole, the ion-exchange between the heavy metal ions and the hydroxyl that bonded with the uncoordinated Cu(II) sites on the adsorbent surface, and the partial reduction of Cr(VI) to Cr(III) during the adsorption of Cr(VI). Generally, pristine MOFs have a lower adsorption capacity for most HMIs than that of modified MOFs. Therefore, coordination interactions mainly occur between HMIs and the modified MOFs with different functional groups (*e.g.*, amino group ($-NH_2$), carboxyl group (–COOH), and thiol group (–SH)). For example, Wang *et al.*[93] compared the FTIR, XPS, X-ray absorption near edge structure (XANES), and extended X-ray absorption fine structure (EXAFS) characterizations of the ZIF-8–PAN nanocomposite before and after adsorption with U(VI) ions and revealed an obvious coordination interaction between the U(VI) ions and the nitrogen atom in 2-methylimidazole.

4. Conclusions and future perspective

In conclusion, MOFs decorated on nanofiber materials have recently achieved substantial progress. A comprehensive review of recent advances in the fabrication of MOFs–nanofiber composites and their applications in removing HMIs from wastewater and aqueous solutions is presented. We focused on two strategies for producing MOF–nanofiber composites: *in situ* MOFs on nanofiber surfaces and pre-synthesized MOF composites. MOFs decorated on nanofiber materials show various attractive adsorbents for removing HMIs, including rapid adsorption kinetics, a high adsorption capacity, excellent selectivity, and good reusability. However, some critical information is missing from the previously published reports. We conclude that the substantial adsorption capacities of MOFs decorated on nanofiber materials are mainly a result of interactions between target ions and functional binding groups on the composites and the highly ordered porous structure that can facilitate the diffusion of metal ions. Despite significant progress, there are still some problems and unresolved issues. In general, experimental conditions such as the pH, ionic strength, competing ions, and organic material significantly influence the surface properties and the adsorption behaviors of HMIs, however, less specific information is available. Another aspect to consider is that the active pH range is often limited (pH 3.0–6.5). Therefore, the stabilization of more MOFs decorated on nanofibers over a wider pH range is very desirable in future studies. As a result, more research is needed into the adsorption behavior of MOFs and the processes of the nanofiber materials that are decorated on the surface as adsorbents. For practical uses of these materials in the control of pollutants, the stability, high adsorption capacity, high selectivity, good reusability, and synthesis by large-scale, inexpensive, and environmentally friendly processes should be considered.

Conflicts of interest

There are no conflicts to declare.

Acknowledgements

The authors are grateful for financial support from USAID Partnerships for Enhanced Engagement in Research (PEER) Program (an international grants program that funds scientists and engineers in developing countries who partner with U.S. government-funded researchers to address global development challenges) and the U.S. National Academies of Sciences Administered Engineering and Medicine (NASEM), PEER/Iraq project/cycle 6. In addition, the authors extend their appreciation to the Deanship of Scientific Research at King Khalid University for funding this work through the research group project under grant number (KKU/RCAMS/G0014/21).

References

1 M. A. Barakat, *Arabian J. Chem.*, 2011, **4**, 361–377.
2 H. Shayegan, G. A. M. Ali and V. Safarifard, *ChemistrySelect*, 2020, **5**, 124–146.
3 E. Khezerloo, S. M. Mousavi-khoshdel and V. Safarifard, *Polyhedron*, 2019, **166**, 166–174.
4 H. Sadegh, G. A. M. Ali, A. S. H. Makhlouf, K. F. Chong, N. S. Alharbi, S. Agarwal and V. K. Gupta, *J. Mol. Liq.*, 2018, **258**, 345–353.
5 B. Dhal, H. N. Thatoi, N. N. Das and B. D. Pandey, *J. Hazard. Mater.*, 2013, **250–251**, 272–291.
6 F. Lu and D. Astruc, *Coord. Chem. Rev.*, 2018, **356**, 147–164.
7 L. N. Nthunya, M. F. Bopape, O. T. Mahlangu, B. B. Mamba, B. Van der Bruggen, C. A. Quist-Jensen and H. Richards, *J. Environ. Manage.*, 2022, **301**, 113922.
8 Z. Lv, C. Liang, J. Cui, Y. Zhang and S. Xu, *RSC Adv.*, 2015, **5**, 18213–18217.
9 L. L. Li, X. Q. Feng, R. P. Han, S. Q. Zang and G. Yang, *J. Hazard. Mater.*, 2017, **321**, 622–628.
10 R. Liang, F. Jing, L. Shen, N. Qin and L. Wu, *J. Hazard. Mater.*, 2015, **287**, 364–372.
11 F. Fu and Q. Wang, *J. Environ. Manage.*, 2011, **92**, 407–418.
12 M. Tanhaei, A. R. Mahjoub and V. Safarifard, *Inorg. Chem. Commun.*, 2019, **102**, 185–191.
13 H. Shayegan, G. A. M. Ali and V. Safarifard, *J. Inorg. Organomet. Polym. Mater.*, 2020, **30**, 3170–3178.
14 H. Sadegh, G. A. M. Ali, V. K. Gupta, A. S. H. Makhlouf, R. Shahryari-ghoshekandi, M. N. Nadagouda, M. Sillanpää and E. Megiel, *J. Nanostruct. Chem.*, 2017, **7**, 1–14.
15 L. Nthunya, M. Masheane, M. George, M.-B. Kime and S. Mhlanga, *J. Water Chem. Technol.*, 2019, **41**, 81–86.
16 B. Makgabutlane, L. N. Nthunya, N. Musyoka, B. S. Dladla, E. N. Nxumalo and S. D. Mhlanga, *RSC Adv.*, 2020, **10**, 2416–2427.
17 L. N. Nthunya, L. Gutierrez, S. Derese, B. B. Mamba, A. R. Verliefde and S. D. Mhlanga, *J. Environ. Chem. Eng.*, 2019, **7**, 103254.

18 G. A. M. Ali, A. Barhoum, V. K. Gupta, A. A. Nada, H. El-Maghrabi, R. Kanthasamy, E. R. Shaaban, H. Algarni and K. F. Chong, *Curr. Nanosci.*, 2020, **16**, 226–234.
19 M. Tanhaei, A. R. Mahjoub and V. Safarifard, *Mater. Lett.*, 2018, **227**, 318–321.
20 O. A. Habeeb, K. Ramesh, G. A. M. Ali and R. M. Yunus, *J. Wuhan Univ. Technol., Mater. Sci. Ed.*, 2017, **32**, 305–320.
21 O. A. Habeeb, K. Ramesh, G. A. M. Ali and R. M. Yunus, *Desalin. Water Treat.*, 2017, **84**, 205–214.
22 L. Esrafili, V. Safarifard, E. Tahmasebi, M. D. Esrafili and A. Morsali, *New J. Chem.*, 2018, **42**, 8864–8873.
23 Z. S. Rozveh, S. Kazemi, M. Karimi, G. A. M. Ali and V. Safarifard, *Polyhedron*, 2020, **183**, 114514.
24 Y. D. Farahani and V. Safarifard, *J. Solid State Chem.*, 2019, **270**, 428–435.
25 L. Zeng, X. Guo, C. He and C. Duan, *ACS Catal.*, 2016, **6**, 7935–7947.
26 C. Y. Sun, C. Qin, X. L. Wang and Z. M. Su, *Expert Opin. Drug Delivery*, 2013, **10**, 89–101.
27 H. Wang, Q. L. Zhu, R. Zou and Q. Xu, *Chem*, 2017, **2**, 52–80.
28 S. Ma and H. C. Zhou, *Chem. Commun.*, 2010, **46**, 44–53.
29 E. Moradi, R. Rahimi and V. Safarifard, *Polyhedron*, 2019, **159**, 251–258.
30 X. Y. Li, Z. J. Li, Y. Z. Li, L. Hou, Z. Zhu and Y. Y. Wang, *Inorg. Chem.*, 2018, **57**, 12417–12423.
31 S. Beheshti, V. Safarifard and A. Morsali, *Inorg. Chem. Commun.*, 2018, **94**, 80–84.
32 Y. Bai, Y. Dou, L. H. Xie, W. Rutledge, J. R. Li and H. C. Zhou, *Chem. Soc. Rev.*, 2016, **45**, 2327–2367.
33 B.-L. Zhang, W. Qiu, P.-P. Wang, Y.-L. Liu, J. Zou, L. Wang and J. Ma, *Chem. Eng. J.*, 2020, **385**, 123507.
34 G. Boix, J. Troyano, L. Garzón-Tovar, C. Camur, N. Bermejo, A. Yazdi, J. Piella, N. G. Bastus, V. F. Puntes, I. Imaz and D. Maspoch, *ACS Appl. Mater. Interfaces*, 2020, **12**, 10554–10562.
35 H.-X. Jin, H. P. Xu, N. Wang, L.-Y. Yang, Y.-G. Wang, D. Yu and X.-K. Ouyang, *Materials*, 2019, **12**, 942.
36 Z. Li, G. Zhou, H. Dai, M. Yang, Y. Fu, Y. Ying and Y. Li, *J. Mater. Chem. A*, 2018, **6**, 3402–3413.
37 G. W. Peterson, D. T. Lee, H. F. Barton, T. H. Epps and G. N. Parsons, *Nat. Rev. Mater.*, 2021, **6**, 605–621.
38 J. Zhao, D. T. Lee, R. W. Yaga, M. G. Hall, H. F. Barton, I. R. Woodward, C. J. Oldham, H. J. Walls, G. W. Peterson and G. N. Parsons, *Angew. Chem., Int. Ed.*, 2016, **55**, 13224–13228.
39 R. Ostermann, J. Cravillon, C. Weidmann, M. Wiebcke and B. M. Smarsly, *Chem. Commun.*, 2011, **47**, 442–444.
40 J. E. Efome, D. Rana, T. Matsuura and C. Q. Lan, *J. Mater. Chem. A*, 2018, **6**, 4550–4555.
41 P. A. Kobielska, A. J. Howarth, O. K. Farha and S. Nayak, *Coord. Chem. Rev.*, 2018, **358**, 92–107.
42 X. Yan, P. Li, X. Song, J. Li, B. Ren, S. Gao and R. Cao, *Coord. Chem. Rev.*, 2021, **443**, 214034.
43 Y. Chen, X. Bai and Z. Ye, *Nanomaterials*, 2020, **10**, 1–23.
44 Z. Li, L. Wang, L. Qin, C. Lai, Z. Wang, M. Zhou, L. Xiao, S. Liu and M. Zhang, *Chemosphere*, 2021, **285**, 131432.
45 H. Yu, S. Gao, X. Cheng, P. Wang, X. Zhang, Y. Xu, H. Zhao and L. Huo, *Sens. Actuators, B*, 2019, **297**, 126744.
46 S. Zhang, J. Wang, Y. Zhang, J. Ma, L. Huang, S. Yu, L. Chen, G. Song, M. Qiu and X. Wang, *Environ. Pollut.*, 2021, **291**, 118076.
47 C. Vaitsis, G. Sourkouni and C. Argirusis, *Ultrason. Sonochem.*, 2019, **52**, 106–119.
48 L. Hu, Y. Huang, F. Zhang and Q. Chen, *Nanoscale*, 2013, **5**, 4186–4190.
49 G. R. Xu, Z. H. An, K. Xu, Q. Liu, R. Das and H. L. Zhao, *Coord. Chem. Rev.*, 2021, **427**, 213554.
50 M. Hao, M. Qiu, H. Yang, B. Hu and X. Wang, *Sci. Total Environ.*, 2021, **760**, 143333.
51 A. Krajnc, B. Bueken, D. De Vos and G. Mali, *J. Magn. Reson.*, 2017, **279**, 22–28.
52 S. R. Venna and M. A. Carreon, *Chem. Eng. Sci.*, 2015, **124**, 3–19.
53 G. H. Albuquerque and G. S. Herman, *Cryst. Growth Des.*, 2017, **17**, 156–162.
54 V. V. Butova, V. A. Polyakov, E. A. Bulanova, M. A. Soldatov, I. S. Yahia, H. Y. Zahran, A. F. Abd El-Rehim, H. Algarni, A. M. Aboraia and A. V. Soldatov, *Microporous Mesoporous Mater.*, 2020, **293**, 109685.
55 A. Schaate, P. Roy, A. Godt, J. Lippke, F. Waltz, M. Wiebcke and P. Behrens, *Chem.–Eur. J.*, 2011, **17**, 6643–6651.
56 J. Yu, C. Mu, B. Yan, X. Qin, C. Shen, H. Xue and H. Pang, *Mater. Horiz.*, 2017, **4**, 557–569.
57 M. H. Yap, K. L. Fow and G. Z. Chen, *Green Energy Environ.*, 2017, **2**, 218–245.
58 V. K. Abdelkader-Fernández, D. M. Fernandes, S. S. Balula, L. Cunha-Silva, M. J. Pérez-Mendoza, F. J. López-Garzón, M. F. Pereira and C. Freire, *ACS Appl. Energy Mater.*, 2019, **2**, 1854–1867.
59 J. Y. Wu, T. C. Chao and M. S. Zhong, *Cryst. Growth Des.*, 2013, **13**, 2953–2964.
60 P. Küsgens, S. Siegle and S. Kaskel, *Adv. Eng. Mater.*, 2009, **11**, 93–95.
61 D. Britt, D. Tranchemontagne and O. M. Yaghi, *Proc. Natl. Acad. Sci. U. S. A.*, 2008, **105**, 11623–11627.
62 C. Liu, Y. N. Wu, C. Morlay, Y. Gu, B. Gebremariam, X. Yuan and F. Li, *ACS Appl. Mater. Interfaces*, 2016, **8**, 2552–2561.
63 E. Laurila, J. Thunberg, S. P. Argent, N. R. Champness, S. Zacharias, G. Westman and L. Öhrström, *Adv. Eng. Mater.*, 2015, **17**, 1282–1286.
64 K. Ma, T. Islamoglu, Z. Chen, P. Li, M. C. Wasson, Y. Chen, Y. Wang, G. W. Peterson, J. H. Xin and O. K. Farha, *J. Am. Chem. Soc.*, 2019, **141**, 15626–15633.
65 X. K. B. Z. F. H. M. S. Shengyang Zhou and X. Chao, *ACS Nano*, 2019, **13**, 9578–9586.
66 A. R. Abbasi, K. Akhbari and A. Morsali, *Ultrason. Sonochem.*, 2012, **19**, 846–852.
67 S. Khanjani and A. Morsali, *Ultrason. Sonochem.*, 2014, **21**, 1424–1429.
68 M. Nakahama, J. Reboul, K. I. Kamei, S. Kitagawa and S. Furukawa, *Chem. Lett.*, 2014, **43**, 1052–1054.

69 A. X. Lu, M. McEntee, M. A. Browe, M. G. Hall, J. B. Decoste and G. W. Peterson, *ACS Appl. Mater. Interfaces*, 2017, **9**, 13632–13636.
70 K. Roongraung, S. Chuangchote, N. Laosiripojana and T. Sagawa, *ACS Omega*, 2020, **5**, 5862–5872.
71 Y. Zhang, S. Yuan, X. Feng, H. Li, J. Zhou and B. Wang, *J. Am. Chem. Soc.*, 2016, **138**, 5785–5788.
72 E. López-Maya, C. Montoro, L. M. Rodríguez-Albelo, S. D. Aznar Cervantes, A. A. Lozano-Pérez, J. L. Cenís, E. Barea and J. A. R. Navarro, *Angew. Chem., Int. Ed.*, 2015, **54**, 6790–6794.
73 M. Nasrabadi, M. A. Ghasemzadeh and M. R. Z. Monfared, *New J. Chem.*, 2019, **43**, 16033–16040.
74 S. Jamshidifard, S. Koushkbaghi, S. Hosseini, S. Rezaei, A. Karamipour, A. Jafari rad and M. Irani, *J. Hazard. Mater.*, 2019, **368**, 10–20.
75 M. R. Thalji, G. A. M. Ali, H. Algarni and K. F. Chong, *J. Power Sources*, 2019, **438**, 227028.
76 W. Tian, H. Zhang, X. Duan, H. Sun, G. Shao and S. Wang, *Adv. Funct. Mater.*, 2020, **30**, 1909265.
77 M. R. Thalji, G. A. M. Ali, P. Liu, Y. L. Zhong and K. F. Chong, *Chem. Eng. J.*, 2021, **409**, 128216.
78 Z. Hu and D. Zhao, *CrystEngComm*, 2017, **19**, 4066–4081.
79 K. Ma, K. B. Idrees, F. A. Son, R. Maldonado, M. C. Wasson, X. Zhang, X. Wang, E. Shehayeb, A. Merhi, B. R. Kaafarani, T. Islamoglu, J. H. Xin and O. K. Farha, *Chem. Mater.*, 2020, **32**, 7120–7140.
80 K. J. Lee, J. H. Lee, S. Jeoung and H. R. Moon, *Acc. Chem. Res.*, 2017, **50**, 2684–2692.
81 Y. T. A. Wong, V. Martins, B. E. G. Lucier and Y. Huang, *Chem.–Eur. J.*, 2019, **25**, 1848–1853.
82 L. Yin, B. Hu, L. Zhuang, D. Fu, J. Li, T. Hayat, A. Alsaedi and X. Wang, *Chem. Eng. J.*, 2020, **381**, 122744.
83 L. N. Nthunya, N. P. Khumalo, A. R. Verliefde, B. B. Mamba and S. D. Mhlanga, *Phys. Chem. Earth, Parts A/B/C*, 2019, **112**, 228–236.
84 J. Huang, Y. Cao, Q. Shao, X. Peng and Z. Guo, *Ind. Eng. Chem. Res.*, 2017, **56**, 10689–10701.
85 L. Peng, X. Zhang, Y. Sun, Y. Xing and C. Li, *Environ. Res.*, 2020, **188**, 109742.
86 J. E. Efome, D. Rana, T. Matsuura and C. Q. Lan, *Sci. Total Environ.*, 2019, **674**, 355–362.
87 J. E. Efome, D. Rana, T. Matsuura and C. Q. Lan, *ACS Appl. Mater. Interfaces*, 2018, **10**, 18619–18629.
88 X. Hou, H. Zhou, J. Zhang, Y. Cai, F. Huang and Q. Wei, *Part. Part. Syst. Charact.*, 2018, **35**, 1–8.
89 N. M. Mahmoodi, M. Taghizadeh, A. Taghizadeh, J. Abdi, B. Hayati and A. A. Shekarchi, *Appl. Surf. Sci.*, 2019, **480**, 288–299.
90 N. D. Shooto, D. Wankasi, L. M. Sikhwivhilu and E. D. Dikio, *J. Residuals Sci. Technol.*, 2016, **13**, 233–242.
91 G. Wang, H. Zhang, J. Wang, Z. Ling and J. Qiu, *Sep. Purif. Technol.*, 2017, **177**, 257–262.
92 R. M. Ashour, A. F. Abdel-Magied, Q. Wu, R. T. Olsson and K. Forsberg, *Polymers*, 2020, **12**, 1–10.
93 C. Wang, T. Zheng, R. Luo, C. Liu, M. Zhang, J. Li, X. Sun, J. Shen, W. Han and L. Wang, *ACS Appl. Mater. Interfaces*, 2018, **10**, 24164–24171.
94 D. Li, X. Tian, Z. Wang, Z. Guan, X. Li, H. Qiao, H. Ke, L. Luo and Q. Wei, *Chem. Eng. J.*, 2020, **383**, 123127.
95 Z. Wei, Q. Su, Q. Lin, X. Wang, S. Long, G. Zhang and J. Yang, *Chem. Eng. J.*, 2022, **430**, 133021.
96 M. Pishnamazi, S. Koushkbaghi, S. S. Hosseini, M. Darabi, A. Yousefi and M. Irani, *J. Mol. Liq.*, 2020, **317**, 113934.
97 G. Zhao, H. Zhao, L. Shi, B. Cheng, X. Xu and X. Zhuang, *Sep. Purif. Technol.*, 2021, **274**, 119054.
98 J. Wen, Y. Fang and G. Zeng, *Chemosphere*, 2018, **201**, 627–643.
99 H. Sadegh, G. A. M. Ali, S. Agarwal and V. K. Gupta, *Int. J. Environ. Res.*, 2019, **13**, 523–531.
100 S. M. Seyed Arabi, R. S. Lalehloo, M. R. T. B. Olyai, G. A. M. Ali and H. Sadegh, *Phys. E Low-dimens. Syst. Nanostruct.*, 2019, **106**, 150–155.